# Active Friction Control in Lubrication Condition Using Novel Metal Morphing Surface

Motoyuki Murashima[*a], Yusuke Imaizumi[*a], Ryo Murase[*a], Noritsugu Umehara[*a], Takayuki Tokoroyama[*a], Toshiyuki Saito[*b], Masayuki Takeshima[*b]

[*a] Department of Micro-Nano Mechanical Science and Engineering, Nagoya University
Furo-cho, Chikusa-ku, Nagoya city, Aichi 464-8603, Japan

[*b] R&D Dept., JTEKT CORPORATION
1-7 Kitajizouyama, Noda-cho, Kariya, Aichi 448-0803, Japan

E-mail address of corresponding author: motoyuki.murashima@mae.nagoya-u.ac.jp

**Abstract**

We propose a new active friction control method with a morphing surface using a unique diaphragm structure consisting of 60-μm thin metal film. In poor lubrication, the friction coefficient dropped significantly from 0.19 to 0.03 when the surface changed from concave to convex. Optical in situ observations revealed that the oil collected at the convexity due to capillary force and meniscus. In addition, results of electric characteristic measurements revealed that the solid contact area decreased with the convexity. In conclusion, the reduction of solid contact due to improvement of lubrication condition was likely the friction reduction mechanism of the convex shape. Because active friction control realizes minimal friction loss and multifunctionality, the morphing surface can contribute to future machine development.

Keywords: metal morphing surface; active friction control; oil collecting; poor lubrication condition

## 1. Introduction

Friction control is an important challenge in tribology engineering. In general, the tribology surfaces of mechanical elements are designed for best performance in steady operations. For example, some surfaces have texturing to reduce friction losses under certain conditions, resulting in better fuel economy and high wear performances [1-10]. On the other hand, a real machine has many operations (e.g., start-up, stop-end, slow speed, and full-power operation) [11,12]. In each operation, tribological conditions (e.g., load, sliding speed, and oil temperature) differ. In addition, because the environment around the machine changes (e.g., temperature, humidity, and vibration), the tribological conditions can differ even with the same operation. Moreover, disturbances (mixing foreign particles, and external shock) also affect tribological conditions. These facts mean that a tribology surface that is optimal for steady operations is not necessarily optimal for the others [13-15]. Here, we consider a tribology surface that actively changes its properties as a future technology for adaptability, high efficiency, energy saving, robustness and multifunctionality [16-22].

In nature, many flora and fauna have unique strategies for survival. Among other things, the surface morphology of living things gives engineers many interesting tips on surface design. The most famous surface in the field of tribology engineering is the lotus leaf [23-27]. The leaf surface has many protrusions covered

by wax, resulting in a superhydrophobic surface. Due to its superhydrophobic nature, water droplets can remove dirt and dust, resulting in a self-cleaning surface. There are other examples of animal and plant skins that exhibit unique properties (e.g., hydrophilicity, low hydrodynamic resistance, strong adhesion, and optical characteristics) [28-34]. Many researchers and engineers are currently attempting to apply micro/nano functional surface morphology to engineering surfaces [35-42].

Another characteristic of living things is their morphing ability. In nature, the environment changes moment to moment. Therefore, flora and fauna must adapt to change. One common strategy for adapting to a changing environment is morphing. For example, raptors fold their wings for high-speed flight in hunting and expand them for long flight [43]. When engineers apply this type of adaptability to machine components, the machine should show better performance in any environment and operating condition. Some morphing technologies are already used in industrial products (i.e., airplanes) [44-48]. However, surface morphing techniques have not yet been applied to tribology surfaces.

Industrial morphing surfaces have many applications in the optical engineering field. Many of them consist of piezoelectric actuators and optical mirrors [49]. The mirror is supported by actuators, which distort the surface morphology of the mirror by pulling or pushing on it. The distortion is used to cancel the optical distortion of the system (i.e., fundus examination), resulting in clear images [50,51]. However, the morphing surfaces are less robust, and are thus not suitable for tribological surfaces.

Ohzono et al. developed a novel morphing surface using the internal stress mismatch of layered material. Wrinkles appear on an elastomer surface covered with a very thin hard coating during compression [52-55]. They found that the amplitude of wrinkles increased with compressive force, and when the force was released, the surface profile returned to flat. The wrinkles were able to transport liquid droplets and microparticles [56,57]. Subsequently, another type of morphing surface was developed using flexible material (i.e., fiber and fabric) to realize friction control [58]. Experimental results showed that the larger the wrinkle amplitude, the higher the friction coefficient, enabling friction control.

Recently, we developed another type of morphing surface, aiming to replace conventional industrial components. Traditionally, morphing tribology surfaces have been composed of elastic material (i.e., rubber, elastomer, and fiber). On the other hand, many mechanical applications need to be made of hard material (i.e., metal, resin and ceramics). In order to realize a morphing surface for practical use, a novel morphing surface made of acrylic resin was developed using additive manufacturing [59]. The surface with a diaphragm structure realizes surface morphing using hard material. The surface achieves a deformation amplitude of 600 μm. Consequently, by morphing, the surface was able to vary its friction coefficient over a wide range (0.3–1.0) under a dry friction condition.

In the present paper, we develop a novel morphing surface using metal material, and clarify its tribological characteristics under oil lubrication. The combination of metal and oil lubricants is widely used in engineering components. Therefore, this new challenge represents the feasibility of morphing surfaces in real products. In addition, the present paper reveals the unique features of the metal morphing surface. In a poor lubrication condition, the convex shape on the surface significantly reduces the friction coefficient. Finally, in

situ optical observations and electrical measurements are used to clarify the unique friction reduction mechanism.

## 2. Experiments

### 2.1. Morphing surface specimen composed of thin metal film

In a previous report, a novel morphing surface was realized using additive manufacturing [59]. Due to the diaphragm structure of the surface, it achieved surface morphing from concave to convex, and vice versa. The method used acrylic resin cured by ultraviolet ray as the manufacturing material because of its flexibility and availability. On the other hand, the resin material showed poor oil resistance due to dissolution in oil. In actual machine operations, many parts are still lubricated with oil. Consequently, the need for a metal morphing surface is urgent.

In the present study, we constructed a metal morphing surface with the diaphragm structure using metal thin film. First, we made a metal base with eight holes (Fig. 1). Subsequently, 60-μm thick aluminum film was glued to the base with epoxy adhesive (Araldaite AR-R30, Huntsman International LLC, U.S.A) (Fig. 2a). The thin film and metal base performed as a diaphragm and supportive structure, the configuration of which has been described in elsewhere [59]. Compressed air was supplied to the metal base, which applied pressure to the backside of the metal film through the holes, leading the thin film to function as a diaphragm structure. As the air pressure on the backside of the diaphragm increased, the diaphragm morphed to a convex shape (Fig. 2b). Similarly, as the pressure decreased to less than atmospheric pressure, the diaphragm shape returned to concave (Fig. 2c). A precision air pressure regulator (RP1000-8-07, CKD corporation, Japan) controlled the pressure loaded to the diaphragm.

A surface profilometer (SV-3100, Mitutoyo Corporation, Japan) was used to measure the diaphragm shape at different backside air pressures from -0.1 to 0.2 MPa (air pressure is described as gauge pressure). The measurement results in Fig. 3 show that the metal morphing surface achieved large transformations of more than 500 μm (from the bottom of the convex shape to the top of the concave shape). The amplitude was the same level as in our previous study, even though the new structure was made of metal. After cyclic deformation (using -0.1 MPa to 0.2 MPa), some plastic deformation (<170 μm) was observed. However, the deformation amplitude was smaller than that of 0.1 MPa (180 μm or more). Therefore, within the range of our experimental conditions, the surface shape returned to the same convex/concave shape when a different pressure was applied. We also made a flat specimen to highlight the performance of the morphing surface. The flat specimen also consisted of thin aluminum film and a metal base except for holes on the base. The root mean square roughness of the aluminum film was $R_q$=0.4 μm.

### 2.2. Friction test

We used a thrust cylinder type friction tester to reveal the tribological properties of the metal morphing surface (Fig. 4). We used a transparent borosilicate glass plate as a mating material to observe contact conditions between the two surfaces. The morphing surface specimen was fixed to a 6-component force sensor

(SFS016XS300U, Leptrino Inc., Japan) onto which a 3-N deadweight was loaded. The force sensor and a specimen holder were connected through a spherical sliding bearing to avoid partial contact between the morphing surface specimen and glass plate. The central axes of rotation of the glass plate and morphing surface specimen were aligned. The arithmetic surface roughness and root mean square roughness of the glass plate was $R_a$=3.2 nm and $R_q$=4.4 nm, respectively.

A speed control motor (SCM315GV-JA, Oriental Motor Co., Ltd., Japan) connected to a gear head (3GV6B, Oriental Motor Co., Ltd., Japan) rotated the rotary table and glass plate through a timing belt. When the glass plate rotated, a friction force was generated by the morphing surface against the glass plate, which was measured by the force sensor. The sensor measured the force as a torque $T$, from which it was possible to calculate a friction force $F$ and friction coefficient $\mu$ using Eq.(1) and Eq.(2) as follows;

$$T = F \cdot r = \mu \cdot W \cdot r \quad (1)$$

$$\mu = \frac{T}{W \cdot r} \quad (2)$$

where $r$ is a radius representing a middle value of the outer and inner radius of the cylinder specimen (19 mm), and $W$ is the normal load.

We also used elastohydrodynamic lubrication (EHL) theory to calculate the film parameter, which is the ratio of oil film thickness to surface roughness. Previously, four types of lubrication mode (i.e., piezoviscous-rigid, piezoviscous-elastic, isoviscous-rigid, isoviscous-elastic) have been proposed, and the contact conditions determine the lubrication mode. The relation between the contact conditions and lubrication modes is described as a lubrication regime map [60]. To determine the lubrication regime of the tribosystem, it is necessary to determine the Young's modulus of the morphing surface. We measured it using a force-displacement curve of the structure, showing a Young's modulus of 30 and 43 MPa at 0.1 and 0.2 MPa, respectively. The lubrication regime map indicates that the lubrication regime of the condition should be in the isoviscous-elastic regime. Therefore, the soft EHL theory is used to calculate the oil film thickness [61].

$$\tilde{H}_{min} = 7.43(1 - 0.85e^{-0.31k})U^{0.65}W^{-0.21} \quad (3)$$

$$\Lambda = \frac{\tilde{H}_{min}}{\sqrt{\sigma_1{}^2 + \sigma_2{}^2}} \quad (4)$$

where $\tilde{H}$ is a minimum-film-thickness, $k$ is the ellipticity parameter, $U$ is a dimensionless speed, $W$ is a dimensionless load parameter, and $\sigma$ is a room mean square roughness of each surface. In our tribosystem, the entrainment velocity shows a positive value depending on the rotation speed of the disc specimen. In addition, the slide-roll-ratio (SRR) shows a value of 2 due to the simple sliding condition. The morphing surface shows the same surface roughness with different shapes. Therefore, the lambda value is calculated using the surface roughness of the aluminum film ($R_q$=0.4 μm) and the glass plate ($R_q$=4.4 nm). In general, the lambda value $\Lambda$ is able to classify lubrication conditions as follows: the boundary lubrication where continuous solid contact occurs ($\Lambda$<1); hydrodynamic lubrication where hydrodynamic pressure separates the two surfaces ($\Lambda$>3);

mixed lubrication where both solid contact and hydrodynamic effects dominate ($1<\Lambda<3$).

We conducted friction tests with varying amounts of oil (from 10–3000 μl) to examine the tribological performance of the morphing surface, especially in a poor lubrication condition. A poly-α-olefin (PAO4) with a viscosity of $9.0\times10^{-3}$ Pa·s at 23 °C was the lubricant oil used in this research. A metallurgical inverted microscope (GX71, Olympus Corporation, Japan) observed the difference in friction state due to morphing. All experiments were conducted in ambient air in a temperature-controlled room at 23 °C.

**3. Low friction in poor lubrication condition with morphing surface**

We conducted various friction tests at a deadweight of 3 N with different sliding speeds (from 30–530 mm/s). The air pressure was increased from 0 to 0.2 MPa by 0.1 MPa per min, and then decreased by 0.1 MPa per min to -0.1 MPa. After the morphing surface changed to a convex shape, it would not return to a concave shape even if the pressure dropped to 0 MPa. Therefore, we used a rotary pump (GVD-050A, ULVAC KIKO Inc., Japan) to reduce the backside pressure to -0.1 MPa, resulting in a concave shape of the diaphragms.

Fig. 5 presents the novel results for active friction control in the oil lubrication condition using the metal morphing surface. The figure shows representative friction curves with varying amounts of oil at a sliding speed of 120 mm/s. In the poor lubrication conditions (10- and 90-μl PAO4), friction coefficients in the first min were around 0.17 with the concave shape. When the morphing diaphragms changed to convex, the coefficient decreased drastically. Subsequently, as convexity increased with the backside air pressure, the coefficient decreased more. In the case of 90-μl PAO4, which showed the lowest friction coefficient in this study, the coefficient decreased from 0.19 to 0.03. This result indicates that the morphing surface was able to achieve 86% friction reduction. In other words, wide-range friction control under a constant operating condition was realized.

In the case of 3000-μl PAO4, at which the oil bath was sufficiently full to totally sink the surface, the friction coefficient in the first min was lower than that for poor lubrication conditions due to better lubrication with enough oil. In addition, friction reduction was also observed with the convexity. However, since the decrease was small, the minimum friction coefficient was 0.06, which was 79% higher than that of the 90-μl condition. This result is interesting because, in general, the better the lubrication condition, the lower the coefficient of friction. Thus, the results should be consistent with the contact and lubrication conditions of the surfaces in contact. We therefore discuss the mechanism in the next section using the in situ surface observation during friction tests.

A morphing surface is able to control a friction coefficient even in a constant sliding condition. In the present research, we changed the sliding speed to investigate the effect of morphing on friction in detail. We varied the sliding speed from 30 to 530 mm/s with different amounts of PAO4 oil.

Figs. 6a-c show the effect of the morphing shape on the friction coefficient with various amount of oil. Figs. 6a, 6b, and 6c display the condition of 10 μl, 90 μl, and 3000 μl, respectively. The morphing surface with the concave shape and the flat specimen typically showed higher friction coefficients compared to convex shapes. In the case of 10 μl, the difference reached up to 0.27 at a sliding speed of 300 mm/s (Fig. 6a). In most

cases, the coefficient decreased as the sliding speed increased in a speed range below 120–200 mm/s, and then the coefficient increased. This tendency matched the theoretical friction prediction with lubricant (i.e., the Stribeck Curve [62-67]), indicating the lubrication condition shifts from the boundary or mixed lubrication condition to a hydrodynamic lubrication condition. The calculated film parameters indicate that the lowest sliding speed (30 mm/s) leads to a lambda value of 0.9 with a concave shape of 0.2 MPa, indicating the boundary lubrication. When the sliding speed reached 60 and 200 mm/s, the values increased to 1.4 and 3.1, respectively. This suggests that mixed and hydrodynamic lubrication occurs at slide speeds of 60–120 mm/s and 200 mm/s and above, respectively. Fig. 7 shows a typical tribological trend; the boundary lubrication shows higher friction (30 mm/s); the coefficient of friction decreases with increasing sliding speed (30–200 mm/s); and the coefficient of friction is dominated by hydrodynamic effects (200–530 mm/s). These results clearly show that the convexity of the morphing surface develops the hydrodynamic effect in the high-speed region even in a poor lubrication condition.

As the amount of lubricant increased, the reduction in the friction coefficient due to morphing decreased, primarily due to improved lubrication for the morphing surface with a concave shape or flat surface. On the other hand, when the surface morphology was convex, especially at 0.2 MPa, the friction coefficient with 90-µl PAO4 showed the lowest value ($\mu$=0.033) despite the smaller amount of lubricating oil compared to 3000 µl ($\mu$=0.061).

Here, we are able to see that the morphing to convex not only reduces the friction coefficient, but also the variation in the friction coefficient (see error bars of plots in Fig. 6). This result also indicates that the convex shape should improve the lubrication condition between surfaces in contact. Fig. 7 shows the effect of convexity on friction with different amounts of oil. In the most severe poor lubrication condition (with 10 µl), the coefficient value was comparably higher except for the case of 3000 µl. For most sliding conditions, oil amounts of 30, 90 and 300 µl produced the lowest friction coefficients. It is interesting that there is an optimal amount of oil (not too much or too little) to realize low friction. The results should be consistent with lubrication conditions and hydrodynamic resistance of the system. Therefore, we discuss these factors in the following sections.

We conducted a 1-hour friction test to examine the wear characteristics of the morphing surface. In the test, the specimen with the convexity of the 0.2-MPa backside pressure was rubbed against the glass disc at a deadweight of 3 N, oil amount of 90-µl, and a sliding speed of 120 mm/s. A 3D measuring laser microscopy (LEXT OLS5000-SAT, Olympus Corporation, Japan) measured a wear volume, and then the wear volume was divided by the normal load and the sliding distance to calculate the specific wear ratio. As a result, the specific wear ratio showed $8.7\times10^{-7}$ mm$^3$/Nm. The value indicates that the contact point of the metal film will be completely worn after 120 hours of friction. In addition, when using a 200-µm thick metal film, it has a durability of 1300 hours or more.

**4. In situ observation of morphing surface**

The advantage of the friction tester we developed is that it enables observation of the contact and

lubrication condition between surfaces in contact. We mainly observed the friction state using the optical microscope system by the contrast of reflectance light.

First, we investigated the effect of the surface morphology on the friction state from the appearance of the friction state. Here, we consider the observation results at a sliding speed of 120 mm/s, oil amount of 90 μl, and a deadweight of 3 N. The lambda value at a sliding speed of 120 mm/s and 0.2 MPa is 2.2, indicating a mixed lubrication region. Fig. 8 shows the spread of oil at the contact point. In the figure, the oi-air boundary is indicated by red dotted lines. When the surface morphology was flat, we could not see a uniform oil film in the flat position (Fig. 8a). Subsequently, when the morphology became convex at 0.2 MPa, the oil collected at the convexity, and the contact position was fully covered by oil (Fig. 8b). In general, convex geometry develops a hydrodynamic pressure facilitating lubrication in the EHL region. The effect plays an important role in reducing friction under lubrication. In addition, Fig. 9 clearly shows that the oil is collected at the contacting point with the convex shape (Fig. 9d) compared to the flat shape (Figs. 9a-c). Due to both effects, the convex shape of the morphing surface provides low and stable friction even in poor lubrication condition. The friction coefficient decreased due to the convex shape even in the boundary lubrication condition (sliding speed of 30 mm/s: $\Lambda$=0.9) (Fig. 6a). These results clearly indicate that not only the hydrodynamic pressure is the only reason, but also the oil collection effect is important to reduce friction in the poor lubrication condition.

Because Fig. 6 suggests that the amount of oil strongly affects the friction coefficient, we conducted in situ optical observations to determine the difference in friction state. At a slow speed of 30 mm/s, the condition with 3000-μl PAO4 showed better oil film with the flat shape (Fig. 9c), whereas the 10-μl condition showed poor oil film (Fig. 9a). The 90-μl PAO4 showed an intermediate state with few air pockets (Fig. 9b). This satisfactory oil film due to the larger amount of oil should prevent solid contact of the surfaces, reducing friction (Fig. 6). However, as discussed in section 3, the friction coefficient with the convex shape showed a different tendency, with a rich oil condition (i.e., 3000 μl) showing the highest coefficient and the 90-μl condition showing the lowest friction (Fig. 7). Fig. 10 shows the difference of the friction state with various amount of oil. The in situ observation revealed that a convex morphology was able to collect a satisfactory amount of oil over the contact area of the convexity regardless of oil amount (Fig. 10a-c). Consequently, every condition showed low friction coefficients (less than 0.061). In the case of hydrodynamic lubrication, the tribosystem is strongly affected by the hydrodynamic resistance against a sliding motion [62-65]. In our research case, the lubrication condition up to 90-μl oil was improved as the amount of oil increased. On the other hand, further increase in oil did not contribute to decreased friction because a sufficient amount of oil was already supplied to the contacting points. Paradoxically, a larger amount of oil increased the hydrodynamic resistance of the system, resulting in an increase of the friction coefficient.

## 5. Measurement of real contact area using electrical characteristics of contacting surface

The in situ observation and friction results suggested that improvement in lubrication condition was the primary reason for the reduction in friction due to morphing. Here, we measured the ratio of the real contact area to the apparent contact area to determine the mechanisms. Subsequently, we demonstrate the effect of the

real contact area on the friction coefficient. In this paper, we call this the breakdown ratio, based on previous studies [68,69]. The parameter was measured using the electrical property of the two surfaces in contact. We used an LCR meter (3522-50, Hioki E.E. Corp., Japan) to measure the electrical properties (i.e., electrical resistance and capacitance). The LCR represents inductance $L$, capacitance $C$, and resistance $R$, and the LCR meter calculates each parameter from the impedance $Z$ measured with an accuracy of 0.08% rdg. In the tests, we used a SUS304 (equivalent to ASTM standard A312) plate (arithmetic surface roughness of $R_a$=9.6 nm) as the conductive material instead of the glass plate. The oil amount and normal load were 30 μl and 3 N, respectively. The measuring and analysis method were developed previously [68,69]. In our test case, we put insulator jigs on the metal base and SUS304 plate to create a closed circuit, and then connected them to the LCR meter.

Fig. 11 shows the breakdown ratios with different surface morphologies. The breakdown ratio for the concave shape at slow speed of 30 mm/s was 36%, and it decreased to 13–14% with convex shapes, resulting in an approximately 73% reduction due to morphing. The friction coefficient also decreased drastically when the surface shape changed from concave to convex. At a speed of 120 mm/s, the breakdown ratio decreased to 6–7% with the convex shape. Fig. 12 clearly shows that the friction coefficient is strongly consistent with the breakdown ratio. Therefore, the reduction of solid contact between two surfaces in contact (i.e., improvement of the lubrication condition) due to the EHL effect (sliding speed of 120 mm/s) and the oil collecting effect (both 30 and 120 mm/s) is likely the mechanism of friction reduction in the convex shape.

Any liquid substance has a certain surface energy (a surface tension) that is the origin of the capillary force and meniscus. In the case of a convex shape contacting a flat surface, the gap gradually narrows toward the tip of the convexity. The narrow gap must generate capillary force and build meniscus of oil due to a balance of surface energies, resulting in oil collecting at the contact points. This must be the origin of the friction reduction using the morphing surface in the boundary lubrication condition. Moreover, the convex shape develops a hydrodynamic pressure, resulting in low friction. The combination of the oil collecting and hydrodynamic effects due to the convexity reduces the friction coefficient even when the tribosystem is in the poor lubrication condition (Fig. 6a).

The previous sections show that too much oil increases the friction coefficient (Fig. 7). That may be because of hydrodynamic resistance due to the viscous force and drag force. Here, we measured hydrodynamic resistance in our tribosystem. To measure the resistance force, we detached the morphing surface slightly from the glass plate (meaning 0 N normal load); the force meter then measured the rotation torque. Fig. 13 contains a modified graph of Fig. 7 by subtracting the hydrodynamic force. As a result, the friction coefficient decreases with a large amount of oil, indicating the friction itself was similar regardless of oil amount. Consequently, the 10-μl condition showed the highest coefficient in most cases.

In conclusion, the present research indicates that the combination of two important factors is important for realizing low friction; one is realizing a hydrodynamic lubrication condition, and the other is reducing hydrodynamic resistance. For the first, the convex morphology can collect lubricant even in a poor lubrication condition. Fig. 14 shows a schematic of the oil collecting effect in a convexity, resulting in an

improved lubrication condition. On the other hand, a flat shape shows a poor lubrication condition due to lack of oil film. Subsequently, the poor lubrication condition shows less hydrodynamic resistance due to the small mass of oil. The metal morphing surface we developed achieved such effective friction reduction due to the unique morphing system consisting of the diaphragm structure. Moreover, the friction control results (wide range of friction coefficients ranging from 0.3–0.03) demonstrate the feasibility of a novel active friction control system that adapts to both the high and low friction required for certain operations.

## 6. Conclusions

The present research shows the friction controllability of the metal morphing surface we created. The morphing surface consisted of 60-μm thick metal thin film and a supportive structure, coupled to form a diaphragm structure. By changing the backside air pressure of the diaphragm, the shape of the diaphragm can change from concave to convex, and vice versa. The amplitude of the morphing reached more than 500 μm, the same level of morphing amplitude as our previous morphing surface made of resin.

In the friction tests lubricated by PAO4 oil, we found that surface morphology strongly affected the friction coefficient. When the surface shape changed to convex, the friction coefficients showed the minimum value in all cases. In addition, the higher the convexity, the lower the coefficient. In the poor lubrication conditions (10 and 90 μl), friction coefficients were around 0.17 with the concave shape. When the morphing parts changed to convex, the coefficient decreased drastically. Subsequently, as the convexity increased with backside air pressure, the coefficient decreased more. In the case of 90-μl lubricant, which showed the best performance in this research, the coefficient decreased from 0.19 to 0.03. This reduction indicates that the morphing surface achieved an 86% reduction of friction. In other words, the surface achieved wide-range friction control in a constant operating condition.

The friction state was observed using an optical microscope through the transparent glass plate, which was the mating material in our friction tests. When the surface shape was flat, we could not see a uniform oil film in the poor lubrication condition. Subsequently, when the morphology changed to convex, the oil collected at the convexity, and the contact area was fully covered by the oil. The in situ observation clearly showed the mechanism of friction reduction due to changes in lubrication condition by morphing.

Finally, we measured the breakdown ratio, which indicates the ratio of a solid contact area to an apparent contact area, by measuring the electrical property of the two surfaces in contact. The breakdown ratio with the concave shape at a slow speed of 30 mm/s was 36%, and decreased to 13–14% with a convex shape, an approximately 73% reduction due to morphing. The friction coefficient also decreased drastically when the surface shape changed from concave to convex. A relation similar to the breakdown ratio to the friction coefficient was observed in the case at 120 mm/s. The statistical analysis clearly showed that the friction coefficient is strongly consistent with the breakdown ratio. Therefore, the reduction of solid contact between two surfaces in contact (i.e., improvement of the lubrication condition) due to oil collecting at the convexity was likely the mechanism of friction reduction with the convex shape. These two findings (i.e., in situ surface observation and breakdown ratio) clearly indicate that the unique morphing method that we propose provides

effective friction control by controlling lubrication conditions.

In conclusion, we clearly showed the novel availability of the metal morphing surface in the present research. The surface is able to maintain low friction by changing its surface morphology. When the amount of lubricant is rich and the operation needs a slow sliding speed, the surface can select a concave shape; when the amount of oil decreases due to long-term operations or external accident, the surface can be changed to a convex shape. This kind of active friction control system is considered important to future machines for fuel efficiency, high performance, personal customized use, and high robustness.

**Declaration of competing interest**

The authors declare that they have no known competing financial interests or personal relationships that could have appeared to influence the work reported in this paper.

**CRediT authorship contribution statement**

**Motoyuki Murashima:** Conceptualization, Methodology, Investigation, Project administration, Resources, Writing – original draft. **Yusuke Imaizumi:** Data curation, Formal analysis. **Ryo Murase**: Data curation, Formal analysis. **Noritsugu Umehara:** Supervision, Writing – review & editing. **Takayuki Tokoroyama:** Methodology, Writing – review & editing. **Toshiyuki Saito:** Methodology, Investigation, Writing – review & editing. **Masayuki Takeshima:** Methodology, Writing – review & editing.

**Acknowledgments**

The authors would like to thank JSPS KAKENHI Grant Number 17K14577, The Hibi Science Foundation, Nagamori Foundation, Research Foundation for the Electrotechnology of Chubu and NSK Foundation for the Advancement of Mechatronics for their financial support.

**References**

[1] Wakuda M, Yamauchi Y, Kanzaki S Yasuda Y. Effect of surface texturing on friction reduction between ceramic and steel materials under lubricated sliding contact. Wear 2003;254:356-63.

[2] Kovalchenko A, Ajayi O, Erdemir A, Fenske G, Etsion I. The effect of laser surface texturing on transitions in lubrication regimes during unidirectional sliding contact. Tribol Int 2005;38:219-25.

[3] Erdemir A. Review of engineered tribological interfaces for improved boundary lubrication. Tribol Int 2005;38:249-56.

[4] Etsion I. Improving tribological performance of mechanical components by laser surface texturing. Tribol Lett 2004;17:733-7.

[5] Kikuchi H, Ibrahim MD, Ochiai M. Evalucation of lubrication performance of foil bearings with new texturing. Tribol Online 2019;14:339-44.

[6] Watanabe K, Seki K, Tadano H, Kaiser F. A study on the friction reduction of seal ring for automatic transmission by applying surface texture. Tribol Online 2017;12:151-4.

[7] Yonehara M, Okubo H, Tadokoro C, Sasaki S, Prakash B. Proposal of biomimetic tribological system to control friction behavior under boundary lubrication by applying 3D metal printing process. Tribol Online 2018;13:8-14.

[8] Tani H, Yamashita N, Koganezawa S, Tagawa N. Taro-leaf inspired patterning of oleophobic surface with high wear resistance. Tribol Online 2018;13:311-5.

[9] Wang X, Kato K, Adachi K, Aizawa K. Loads carrying capacity map for the surface texture design of SiC thrust bearing sliding in water. Tribol Int 2003;36:189-97.

[10] Oyama S, Umehara N, Kousaka H, Deng X, Murashima M, Horie S, Matsuyama Y. Effect of drill surface texturing on back burr height with solid lubricating sheet in titanium alloy drilling. Trans JSME (in Japanese) 2017;83:1-10.

[11] Holmberg K, Andersson P, Erdemir A. Global energy consumption due to friction in passenger cars. Tribol Int 2012;42:221-34.

[12] Holmberg K, Kivikyö-Reponen P, Härkisaari P, Valtonen K, Erdemir A. Global energy consumption due to friction and wear in the mining industry. Tribol Int 2017;115:116-39.

[13] Etsion I, Sher E, Improving fuel efficiency with laser surface textured piston rings. Tribol Int 2009;42:542-7.

[14] Borghi A, Gualtieri E, Marchetto D, Moretti L, Valeri S, Tribological effects of surface texturing on nitriding steel for high-performance engine applications. Wear 2008;265:1046-51.

[15] Yu H, Wang X, Zhou F. Geometric shape effects of surface texture on the generation of hydrodynamic pressure between conformal contacting surfaces. Tribol Lett 2010;37:123-30.

[16] Pilkington GA, Haris K, Bergendal E, Reddy AB, Palsson GK, Vorobiev A, Antzutkin ON, Glavatskih S, Rutland MW. Electro-responsivity of ionic liquid boundary layers in a polar solvent revealed by neutron reflectance. J Chem Phy 2018;148:193806-1-9.

[17] Hjalmarsson N, Bergendal E, Wang YL, Munavirov B, Mallinder D, Glavatskih S, Aastrup T, Atkin R, Furó I, Rutland MW. Electro-responsive surface composition and kinetics of an ionic liquid in a polar oil. Langmuir 2019;35:15692-15700.

[18] Murashima M, Umehara N, Kousaka H. Effect of alternating electric field intensity on adhesion of thermoplastic resin. Proc 6th Int Conf Mech Mater Des 2015:335-338.

[19] Murashima M, Umehara N, Kousaka H, Deng X. Effect of electric field on adhesion of thermoplastic resin against steel plate. Tribol Online 2017;12:42-8.

[20] Tokoroyama T, Kamiya M, Umehara N, Wang C, Diao D. Influence of UV irradiation in low frictional performance of CNx coatings. Lubr sci 2012;24:129-39.

[21] Taib MTB, Umehara N, Tokoroyama T, Murashima M. The effect of UV irradiation to a-C:H on friction and wear properties under PAO oil lubrication including MoDTC and ZnDTP. Tribol Online 2018;13:119-30.

[22] Murashima M, Oh SJ, Miyachi T, Umehara N, Tokoroyama T, Konishi K, Okamoto T. Proposal of development guidline for low frictional material in oil lubrication with high permittivity material. Proc

6th Int Conf Integrity-reliability-Failure 2018:941-942.
[23] Barthlott W, Neinhuis. Purity of the sacred lotus, or escape from contamination in biological surfaces. Planta 1997;202:1-8.
[24] Feng L, Li S, Li Y, Li H, Zhang L, Zhai J, Song Y, Liu B, Jiang L, Zhu D. Super-hydrophobic surfaces: From natural to artificial. Adv Mater 2002;14:1857-60.
[25] Neinhuis C, Barthlott W. Characterization and distribution of water-repellent, self-cleaning plant surfaces. Annu Botany 1997;79:667-77.
[26] Quéré D. Wetting and roughness. Annu Rev Mater Res 2008;38:71-99.
[27] Roach P, Shirtcliffe NJ, Newton MI. Progress in superhydrophobic surface development. Soft Matter 2008;4:224-40.
[28] Sekiguchi A, Matsumoto Y, Minami H, Nishino T, Tanigawa H, Tokumaru K, Tsumori F. Study of the antifouling polymer sheet which used biomimetics technique. J Photopolymers Sci Technol 2018;31:121-8.
[29] Oeffner J, Lauder GV. The hydrodynamic function of shark skin and two biomimetic applications. J Exp Biol 2012;215:785-95.
[30] Autumn K, Liang YA, Hsieh ST, Zesch W, Chan WP, Kenny TW, Fearing R, Full RJ. Adhesive force of a single gecko foot-hair. Nature 2000;405:681-5.
[31] Wilson SJ, Hutley MC. The optical properties of 'moth eye' antireflection surfaces. Opt Acta 1982;29:993-1009.
[32] Huang J, Wang X, Wang ZL. Controlled replication of butterfly wings for achieving tunable photonic properties. Nano Lett 2006;6:2325-31.
[33] Vukusic P, Sambles JR, Lawrence CR, Wootton RJ. Quantified interference and diffraction in single morpho butterfly scales. Proc R Soc Lond B 1999;266:1403-11.
[34] Kinoshita S, Yoshioka S, Miyazaki J. Physics of structural colors. Rep Prog Phys 2008;71:1-30.
[35] Feng X, Jiang L. Design and creation of superwetting/Antiwetting surfaces. Adv Mater 2006;18:3063-78.
[36] Murashima M, Umehara N, Kousaka H. Effect of nano-texturing on adhesion of thermoplastic resin against textured steel plate. Tribol Online 2016;11:159-67.
[37] Wen L, Weaver JC, Lauder GV. Biomimetic shark skin: design, fabrication and hydrodynamic function. J Exp Biol 2014;217:1656-66.
[38] Geim AK, Dubonos SV, Grigorieva IV, Novoselov KS, Zhukov AA, Shapoval SYU. Microfabricated adhesive mimicking gecko foot-hair. Nature Mater 2003;2:461-3.
[39] Kaless A, Schulz U, Munzert P, Kaiser N. Nano-motheye antireflection pattern by plasma treatment of polymers. Surf Coat Technol 2005;200:58-61.
[40] Behera S, Joseph J. Single-step optical realization of bio-inspired dual-periodic motheye and gradient-index-array photonic structures. Opt Lett 2016;41:3579-82.
[41] Song, YM, Xie Y, Malyrchuk V, Xiao J, Jung I, Choi KJ, Liu Z, Park H, Lu C, Kim RH, Li R, Crozier KB, Huang Y, Rogers J. Digital cameras with designs inspired by the arthropod eye. Nature 2013;497:95-

99.
[42] Clapham PB, Hutley MC. Reduction of lens reflexion by the moth eye principle. Nature 1973;244:281-2.
[43] Tucker VA, Parrott GC. Aerodynamics of gliding flight in a falcon and other birds. J Exp Biol 1970;52:345-67.
[44] Weisshaar TA. Morphing aircraft technology – new shapes for aircraft design. NATO OTAN 2006;RTO-MP-AVT-141:1-20.
[45] Weisshaar TA. Morphing aircraft systems: Historical perspectives and future challenges. J Aircraft 2013;50:337-353.
[46] Barbarino S, Bilgen O, Ajaj RM, Friswell MI, Inman DJ. A review of morphing aircraft. J Intel Mater Syst Struct 2011;22:823-55.
[47] Meguid SA, Su Y, Wang Y. Complete morphing wing design using flexible-rib system. Int J Mech Mater Des 2017;13:159-71.
[48] Thill C, Etches JA, Bond IP, Potter KD, Weaver PM. Composite corrugated structures for morphing wing skin applications. Smart Mater Struct 2010;19:1-10.
[49] Bifano TG, Perreault J, Mali RK, Horenstein MN. Microelectromechanical deformable mirrors. IEEE J Selec Topi Quant Electronics 1999;5:83-89.
[50] Zeek E, Maginnis K, Backus S, Russek U, Murnane M, Mourou G, Kapteyn H. Pulse compression by use of deformable mirrors. Opt Lett 1999;24.493-495.
[51] Sherman L, Ye JY, Albert O, Norris TB. Adaptive correction of depth-induced aberrations in multiphoton scanning microscopy using a deformable mirror. J Microscopy 2002;206:65-71.
[52] Ohzono T, Shimomura. Ordering of microwrinkle patterns by compressive strain. Phy Rev B 2004;69:132202-1-4
[53] Ohzono T, Shimomura M. Geometry-dependent stripe rearrangement processes induced by strain on preordered microwrinkle patterns. Langmuir 2005;21:7230-7.
[54] Ohzono T, Watanabe H, Vendamme R, Kamaga C, Kunitake T. Spatial forcing of self-organized microwrinkles by periodic nanopatterns. Adv Mater 2007;19:3229-32.
[55] Ohzono T, Monobe, H, Shiokawa K, Fujiwara M, Shimizu Y. Shaping liquid on a micrometer scale using microwrinkles as deformable open channel capillaries. Soft Matter 2009;5:4658-64.
[56] Ohzono T, Monobe H, Yamaguchi R, Shimizu Y, Yokoyama H. Dynamics of surface memory effect in liquid crystal alignment on reconfigurable microwrinkles. Appl Phy Lett 2009;95:014101-1-3.
[57] Ohzono T, Fukuda JI. Zigzag line defects and manipulation of colloids in a nematic liquid crystal in microwrinkle grooves. Nature comm 2012;3:1-7.
[58] Suzuki K, Ohzono T. Wrinkles on a textile-embedded elastomer surface with highly variable friction. Soft Matter 2016;12:6176-6183.
[59] Murashima M, Yoshino S, Kawaguchi M, Umehara N. Intelligent tribological surfaces: from concept to realization using additive manufacturing. Int J Mech Mater Des 2019;15:757-66.
[60] Hamrock BJ, Dowson D. Ball bearing lubrication : the elastohydrodynamics of elliptical contacts. John

Wily & Sons 1981.
[61] Hamrock BJ, Dowson D. Elastohydrodynamic lubrication of elliptical contacts for materials of low elastic modulus I - fully flooded conjunction. J Lubr Technol 1978;100:236-245.
[62] Jacobson B. The Stribeck memorial lecture. Tribol Int 2003;36:781-9.
[63] Lu X, Khonsari MM, Gelinck ERM. The Stribeck curve: experimental results and theoretical prediction. J Tribol 2006;128;789-94.
[64] Gelinck ERM, Schipper DJ. Calculation of Stribeck curves for line contacts. Tribol Int 2000;33:175-81.
[65] Kraker AD, Ostayen RAJ, Rixen DJ. Calculation of Stribeck curves for (water) lubricated journal bearings. Tribol Int 2007;40:459-69.
[66] Kovalchenko A, Ajayi O, Erdemir A, Fenske G, Etsion I. The effect of laser surface texturing on transitions in lubrication regimes during unidirectional sliding contact. Tribol Int 2005;38:219-25.
[67] Lu X, Khonsari MM. An experimental investigation of dimple effect on the Stribeck curve of journal bearings. Tribol Lett 2007;27:169-76.
[68] Maruyama T, Nakano K. In situ Quantification of oil film formation and breakdown in EHD contacts. Tribol Trans 2018;61:1057-66.
[69] Maruyama T, Maeda M, Nakano K. Lubrication condition monitoring of practical ball bearings by electrical impedance method. Tribol Online 2019;14:327-38.

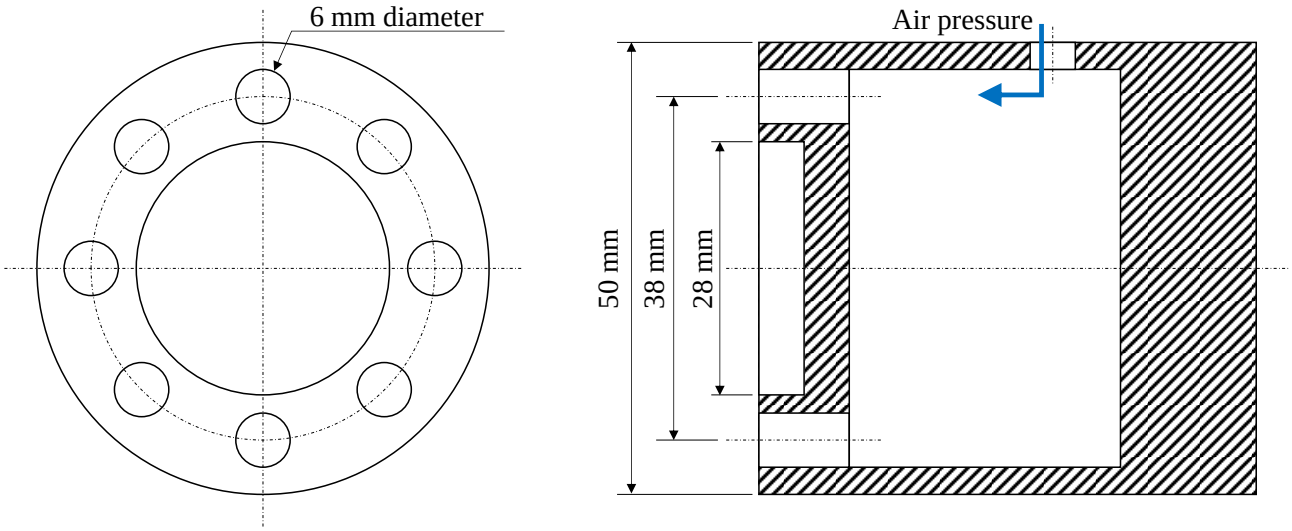


Fig. 1 A drawing of the metal base. Thin metal film was glued on the left side of the side view (right).

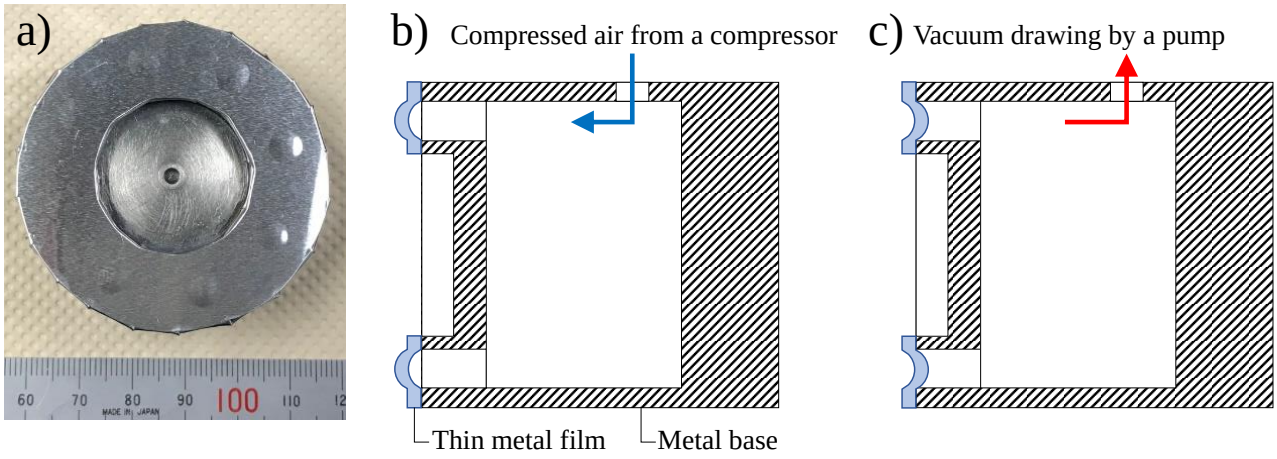


Fig. 2 (a) Photo image, and cross-section schematics of the metal morphing surface specimen with (b) convex and (c) concave shape.

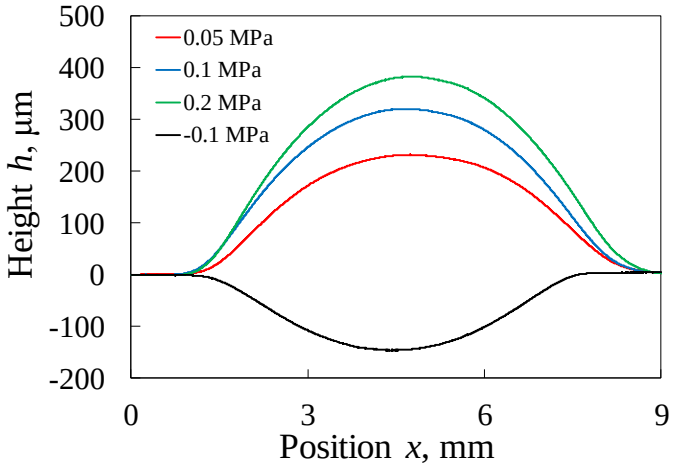


Fig. 3 The diaphragm shapes at different backside air pressure values.

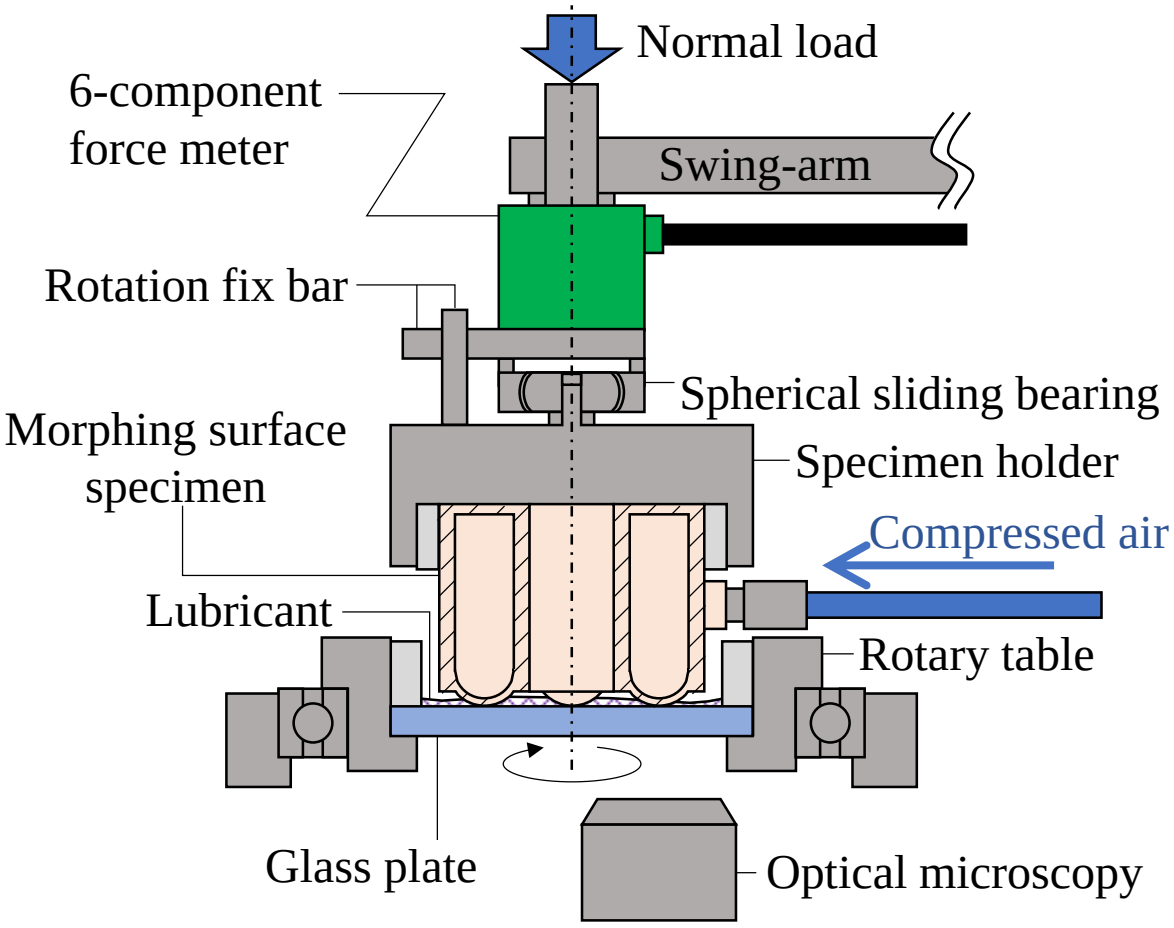


Fig. 4 A schematic of the thrust cylinder type friction tester. The rotation fix bar stops the rotation of the cylinder specimen and transmits the friction torque to the force meter.

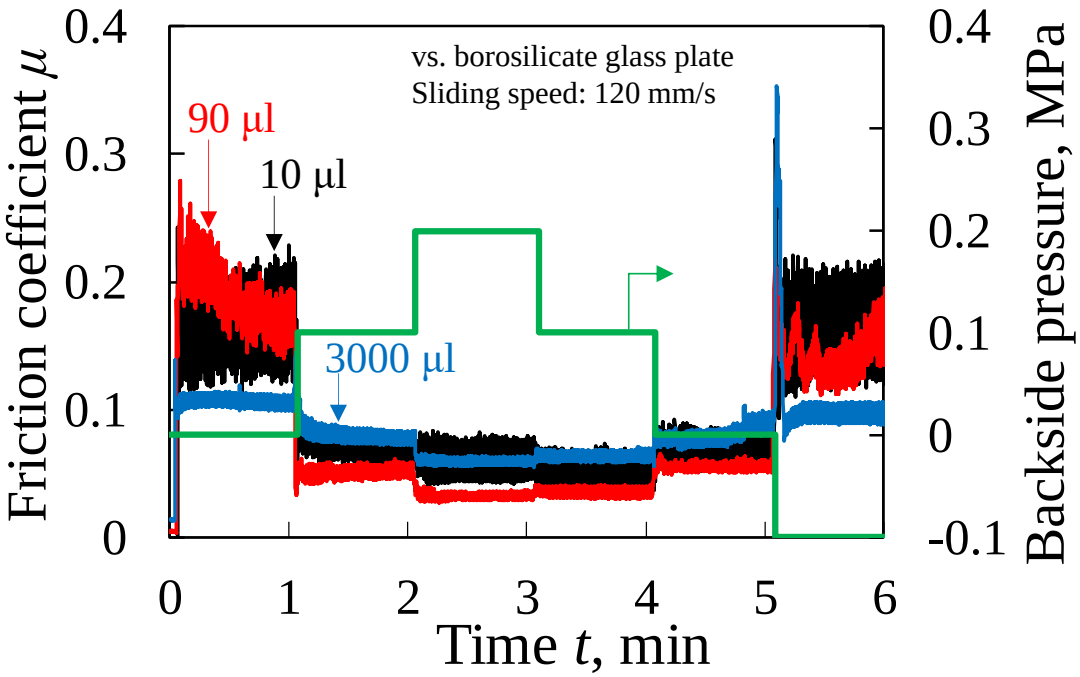


Fig. 5 Friction coefficients of the metal morphing surface with different amounts of oil at a sliding speed of 120 mm/s.

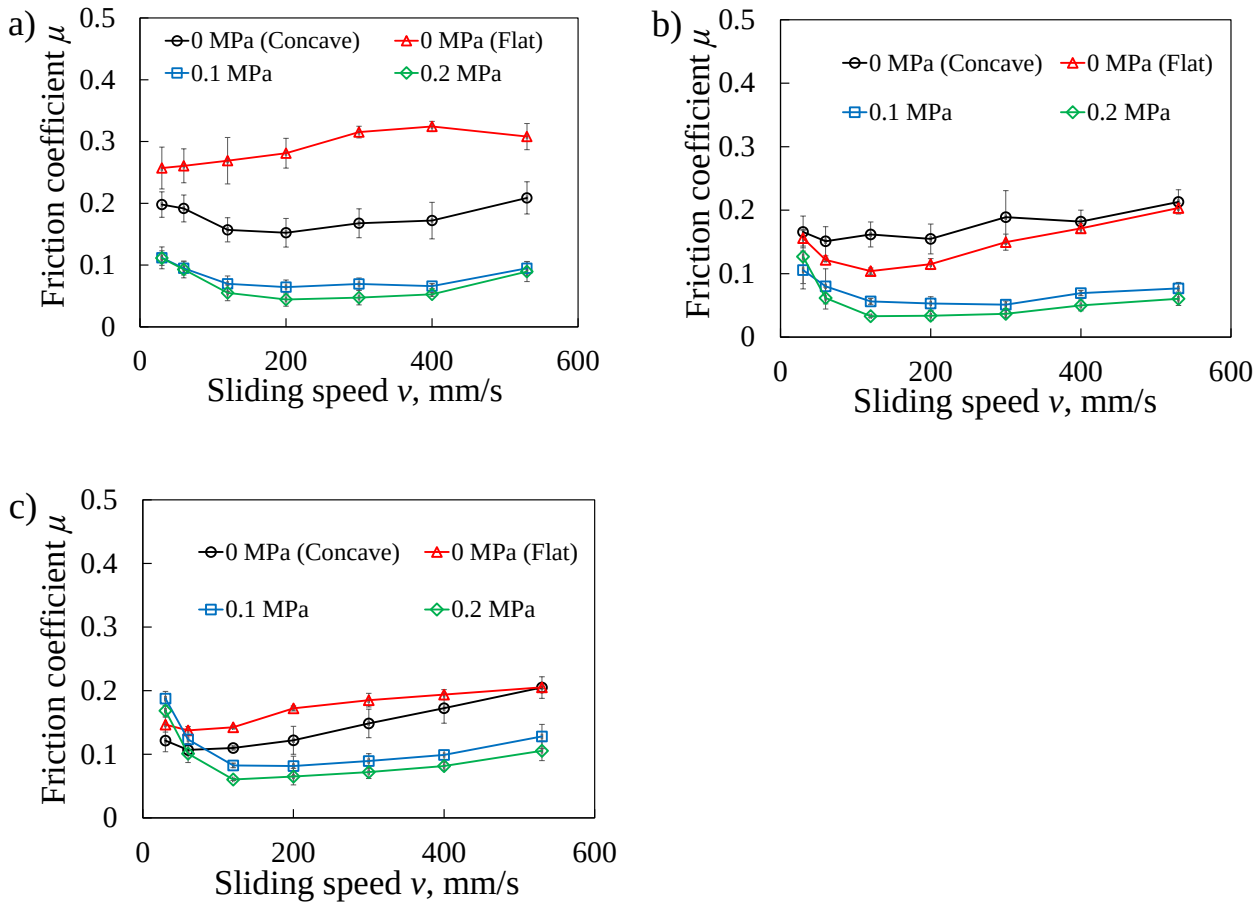


Fig. 6 Friction coefficients at different sliding speeds with varieties of surface morphology under oil lubrication condition of: (a) 10 μl, (b) 90 μl, and (c) 3000 μl.

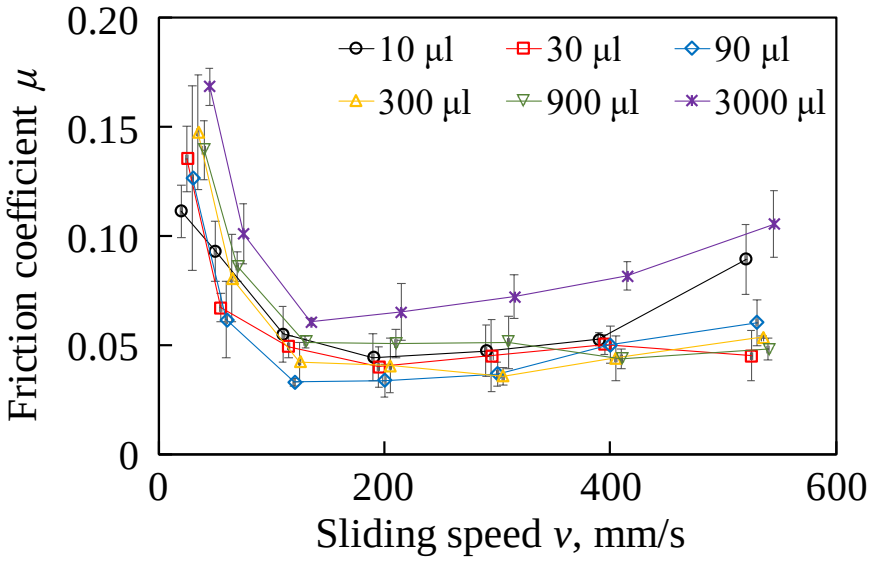


Fig. 7 Friction coefficients at different sliding speeds with the convex morphology at 0.2 MPa backside pressure. The plotted points are slightly shifted along the x-axis by the amount of lubricant for visibility (the 90-μl line shows the correct value in sliding speed).

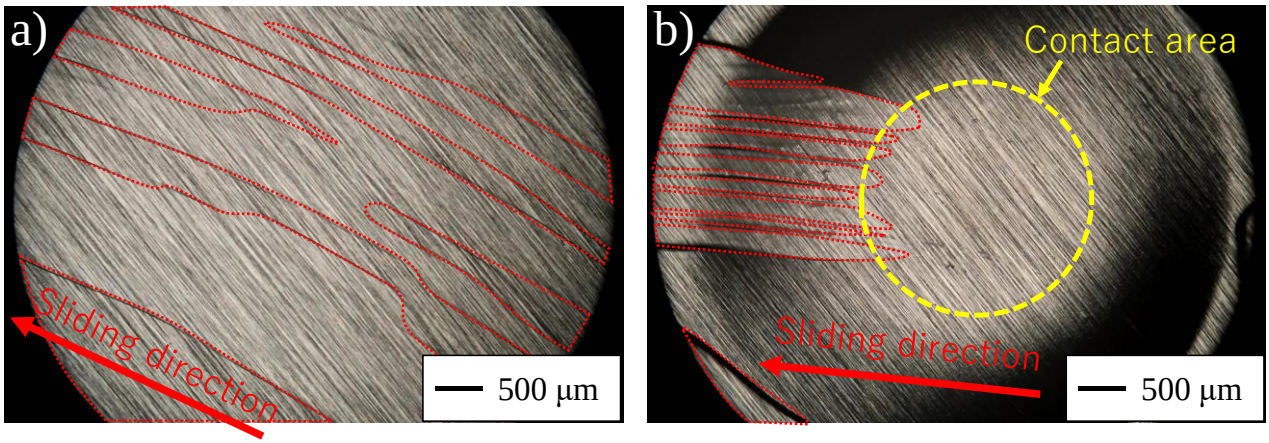


Fig. 8 The friction state of (a) flat and (b) convex shape at sliding speed of 120 mm/s and 90 µl of oil. The red dotted lines indicate the boundary between oil and air.

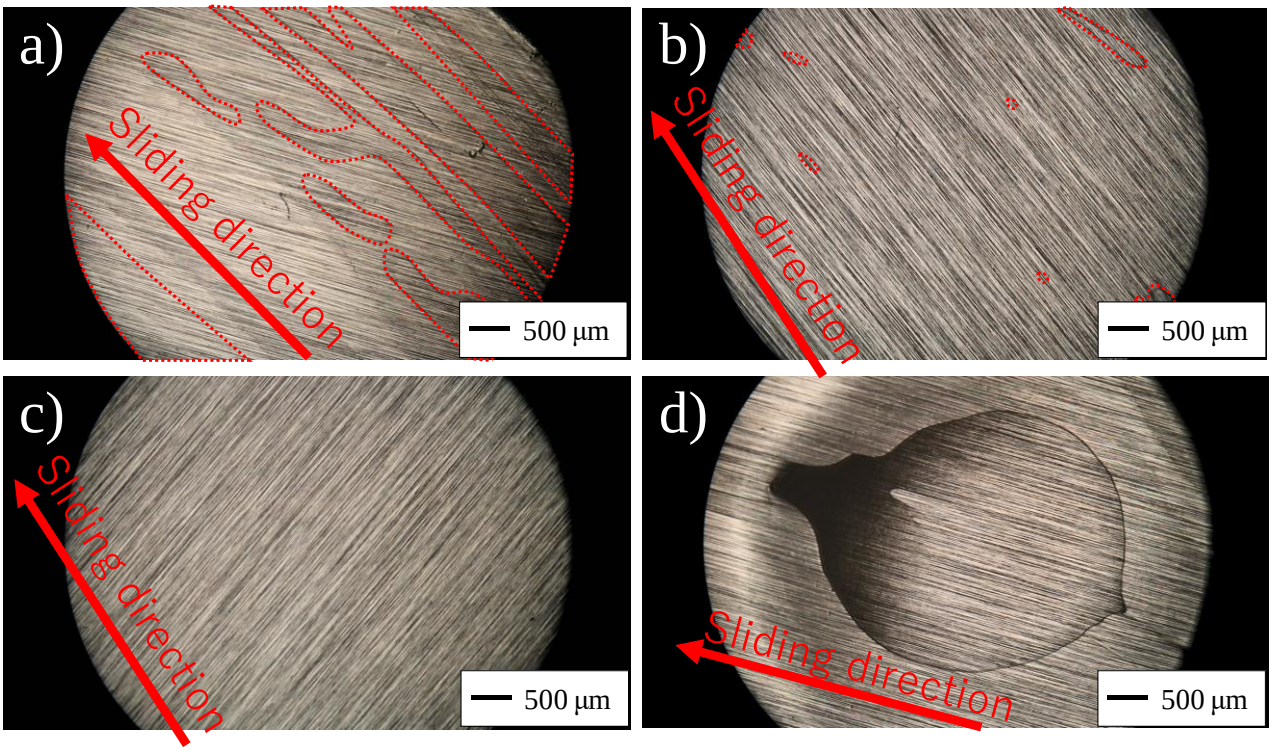


Fig. 9 The differences of the friction state at a sliding speed of 30 mm/s with the flat surface with oil amounts of: (a) 10 µl, (b) 90 µl, and (c) 3000 µl. And (d) the friction state with the convex shape at 0.2 MPa and 10-µl oil is also shown. The red dotted lines indicate the boundary between oil and air.

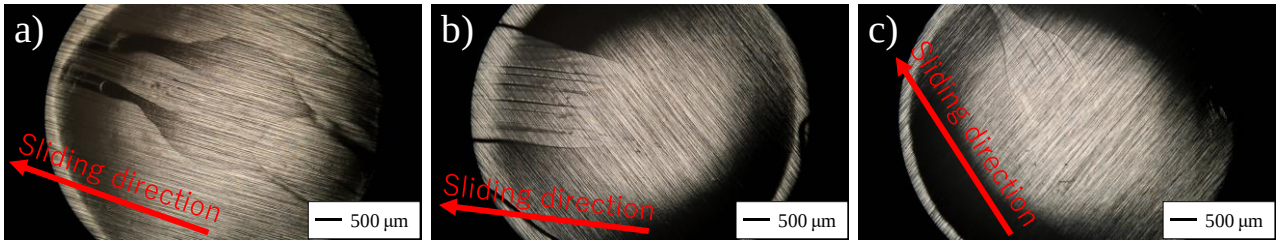


Fig. 10 The differences of the friction state at a sliding speed of 120 mm/s with the convexity of 0.2 MPa in oil amounts of: (a) 10 µl, (b) 90 µl, and (c) 3000 µl.

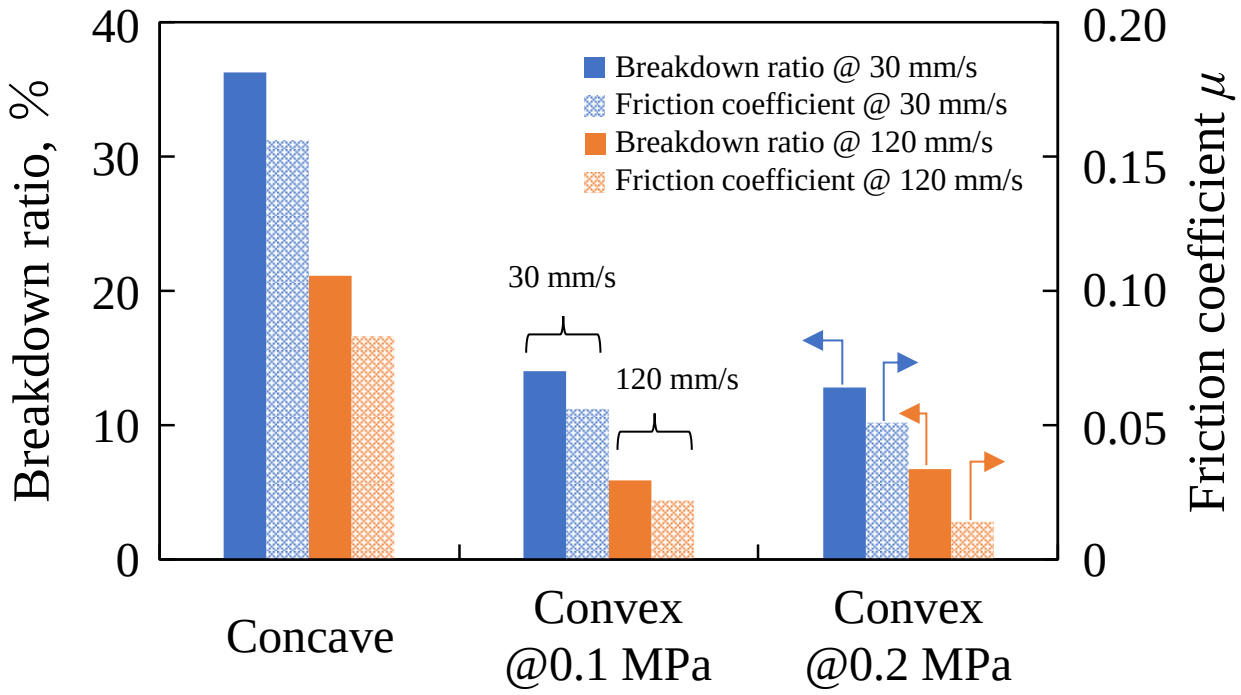


Fig. 11 The breakdown ratio with different surface morphology. Every value is the average of last 30 sec during the friction test. The normal load of 3 N and sliding speed of 30 or 120 mm/s was used in the friction test.

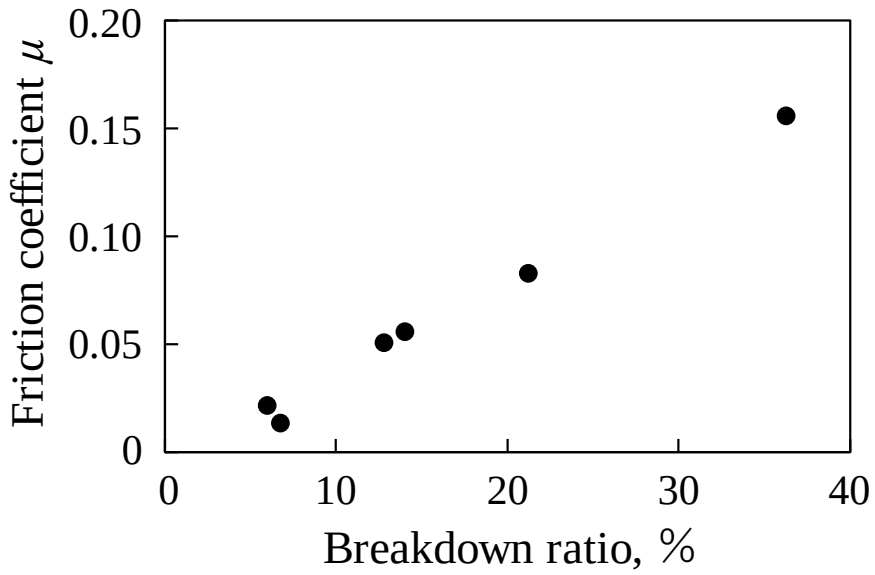


Fig. 12 The decrease in the friction coefficient with breakdown ratio. The normal load of 3 N and sliding speed of 30 or 120 mm/s was used in the friction test.

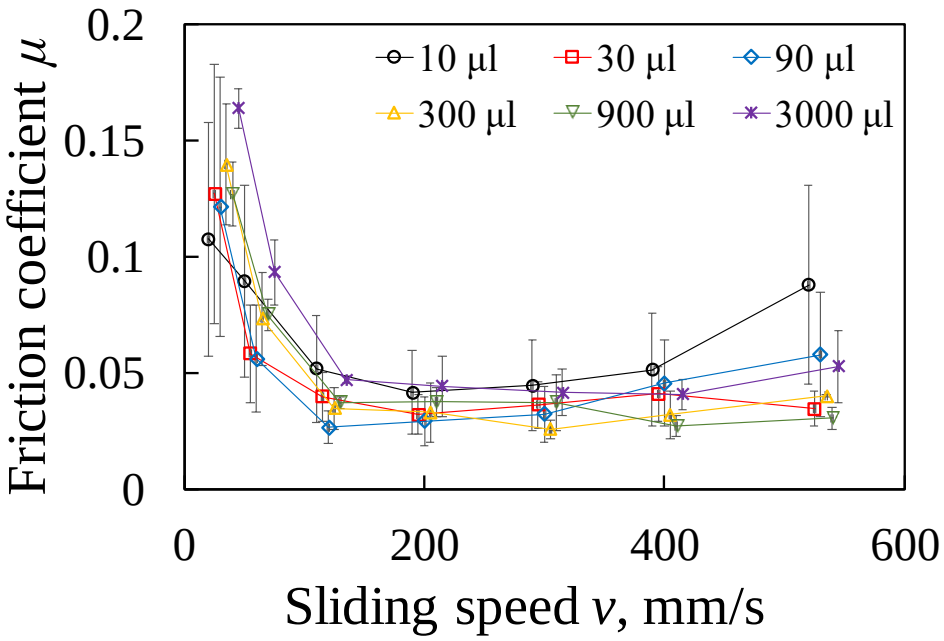


Fig. 13 Friction coefficient obtained by subtracting hydrodynamic resistance from the friction coefficient shown in Fig. 7 (convex shape). The plotted points are slightly shifted along the x-axis by the amount of lubricant for visibility (the 90-μl line shows the correct value of sliding speed).

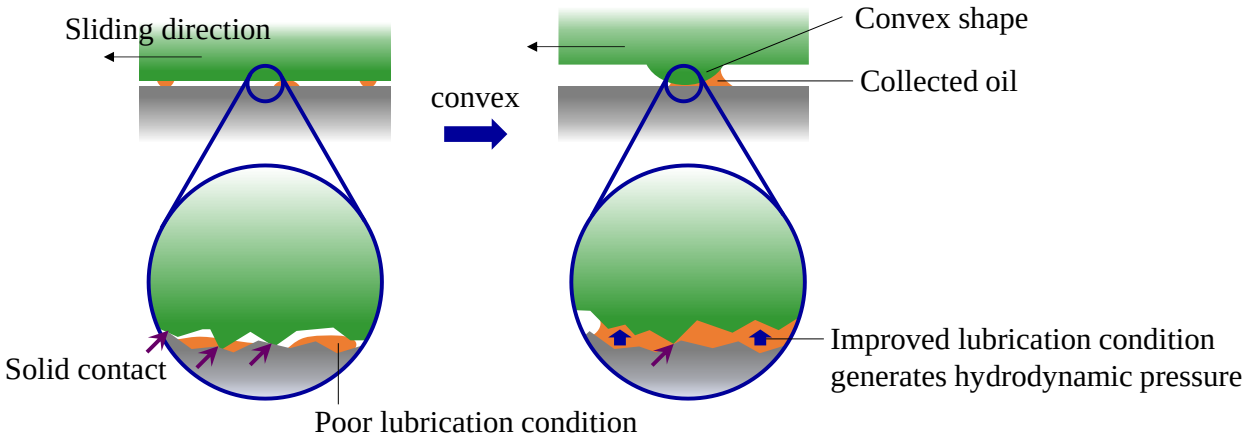


Fig. 14 Schematics of the friction reduction mechanism due to collection of oil with convex shape and hydrodynamic effect.